Crystalline ZnO/Amorphous ZnO Core/Shell Nanorods: Self-Organized Growth, Structure and Novel Luminescence

Saikumar Inguva [1], Sandeep Kumar Marka [2], Rajani K. Vijayaraghavan [3], Enda McGlynn [1], Vadali.V.S.S. Srikanth [2], J.-P. Mosnier [1].*

[1]School of Physical Sciences and National Centre for Plasma Science and Technology, Dublin City University, Glasnevin, Ireland.

[2]School of Engineering Sciences and Technology, University of Hyderabad, Hyderabad 500046, India.

[3]School of Electronic Engineering and National Centre for Plasma Science and Technology, Dublin City University, Glasnevin, Ireland.

*jean-paul.mosnier@dcu.ie

KEYWORDS

ZnO, core/shell, nanorod, pulsed laser deposition, defects, photoluminescence

ABSTRACT

We have used pulsed-laser deposition, following a specific sequence of heating and cooling phases, to grow ZnO nanorods on ZnO buffer/Si (100) substrates, in a 600 mT oxygen ambient, without catalyst. In these conditions, the nanorods preferentially self-organize in the form of vertically aligned, core/shell structures. X-ray diffraction analyses, obtained from 2θ-ω and pole figure scans, shows a crystalline (wurtzite) ZnO deposit with uniform *c*-axis orientation normal to the substrate. Field emission SEM, TEM, HR-TEM and selective area electron diffraction (SAED) studies revealed that the nanorods have a crystalline core and an amorphous shell. The low-temperature (13 K) photoluminescence featured a strong I_6 (3.36 eV) line emission, structured green band emission and a hitherto unreported broad emission at 3.331 eV. Further studies on the 3.331 eV band showed the involvement of deeply-bound excitonic constituents in a single electron-hole recombination. The body of structural data suggests that the 3.331 eV emission can be linked to the range of defects associated with the unique crystalline ZnO/amorphous ZnO core/shell structure of the nanorods. The relevance of the work is discussed in the context of the current production methods of core/shell nanorods and their domains of application.

1. Introduction

Core/shell nanostructures constituted by a variety of materials including metals,[1] semiconductors,[2-4] hydroxides,[5] and organic materials[6] have been attracting significant attention for applications in several interdisciplinary fields such as sensing, multi-enzyme bio-catalysis, drug delivery and photonics, for example.[7] This is because the core/shell architecture enables the tailoring of novel properties via modification of the functionality, charge or reactivity of the nanostructures surface.[2-4,8] In particular, the enhancement of the luminescent properties of one-dimensional nanostructures can be achieved following this method.[8]

ZnO, a wide direct band gap (3.37 eV) semiconductor, has been used successfully in core/shell architectures due to its excellent material properties[9-11] that include relatively facile nanostructure fabrication. ZnO based core/shell nanostructures including ZnO/Fe_2O_3, ZnO/In_2O_3,[12,13] ZnO/ZnS, ZnO/ZnTe, ZnO/TiO_2,[14-17] ZnO/MoO_3, hydrogenated ZnO,[18,19] and ZnO/NiO[20] have been produced for applications in gas sensors, photovoltaics, super capacitors and energy storage, respectively. In this context, ZnO/Bi_2O_3,[21] Zn/ZnO,[22,23] and ZnO/$ZnO(OH)_2$[24] core/shell architectures have also been reported.

Core/shell nanostructures are typically fabricated as part of complex multi-step processes. In the first step, the nanostructure core is fabricated, followed by the growth of the shell region in a second step, with several intermediate operations and possibly a change of growth method being implemented between these two steps. For example, Greene et al. have fabricated ZnO nanorod core in a two-step aqueous process and subsequently prepared a TiO_2 shell by atomic layer deposition.[15] Huang et al. have fabricated the ZnO core and In_2O_3 shell by aqueous chemical process and a combination of sputtering and thermal oxidation methods, respectively.[13]

Additionally, other growth methods such as hydrolysis,[12,16] electro-chemical,[18] and pulsed laser deposition (PLD)[8,25] have been used by other workers. Of particular interest for the present work, we note the PLD works of Kaydashev et al.[25] and Li et al.[8] who prepared ZnO/$Zn_{0.9}Mn_{0.1}O$ and ZnO/Er_2O_3 core/shell nanorods using multi-step growth processes in Ar and/or O_2 ambient pressures with the aid of Au-catalyst, respectively.

In this work, we develop a specific catalyst free- PLD growth sequence to obtain self-organized ZnO/ZnO core/shell nanorods without the need for a separate growth step for the shell, using as the substrate a Si (100) wafer coated by a thin ZnO buffer layer. We also investigate the structural, morphological and optical properties of the as-grown ZnO/ZnO core/shell nanorod deposit and the relationship of the latter to the unique defect structure associated with the core/shell architecture.

2. Experimental details

ZnO/ZnO core/shell nanorods were grown using a standard PLD apparatus equipped with a high-power, Q-switched, frequency-quadrupled, Nd:YAG laser.[26] The output laser wavelength, repetition rate, pulse width and energy were 266 nm, 10 Hz, 6 ns and 150 mJ, respectively. The average fluence delivered at the laser spot was ~ 2.0 J/cm^2. ZnO (99.999% pure, PI-KEM) sintered ceramic disk of diameter 2.54 cm was used as the target. The target-substrate distance was kept constant at 5 cm. Cleaved 1 cm × 2 cm pieces of Si (100) wafers were used as substrates. Prior to deposition, the substrates were degreased/cleaned for 15 minutes in an ultrasonic bath filled with acetone/isopropyl alcohol. Silver paste was used to mount substrates on the substrate holder in the deposition chamber. Before deposition, the substrates were heated

to 900 °C for 30 minutes for the purpose of surface cleaning using a heater coil and then cooled down to 450 °C.

The fabrication of ZnO/ZnO core/shell nanorods on Si (100) wafer substrates involved two stages. The first stage was to prepare a thin ZnO buffer layer. The buffer layer of thickness around 120 nm (5000 laser shots) was deposited at a substrate temperature of 450 °C in an ambient O_2 pressure of 100 mT. Following deposition of the buffer layer, the substrate temperature was increased to 700 °C at a rate of 12.5 °C /minute, then left at this temperature for 5 minutes, and finally cooled down to 150 °C at a rate of 9.16 °C /minute. The second stage involved the preparation of the core/shell nanorods. The ZnO buffer/substrate temperature was initially raised to 800 °C at a rate of 7.22 °C/minute. The ZnO/ZnO core/shell nanorods were then grown at this temperature in a 600 mT O_2 pressure and left in these conditions for 5 minutes. After this period, the substrate temperature was cooled down to 150 °C at a rate of 8.66 °C/minute. The actual deposition time of the core/shell nanorods was about 2 hrs (40,000 laser shots), excluding the sequence of heating and cooling phases to pre- and post-growth. The full length of the core/shell nanorod obtained in these conditions was around 1 μm**.** Five growths using the same conditions and sequences were performed. The same nanorod architecture was obtained in each case and is thus fully reproducible. From the viewpoint of the growths, we conclude that the overall sequence of specific heating and cooling phases used in this work has allowed us to achieve self-organized core/shell architecture, without the need for a separate growth step for the shell region. The self-organization of ZnO nanostructures is a known feature of this material.[27] Also, to the best of our knowledge, similar growths of ZnO nanorods[28,29] carried out in similar pressure conditions, all lead to a simple nanorod structure, i.e. without a shell. Thus, we can conclude that the series of substrate temperatures for the given deposition

rate used in this PLD work should be the important parameter influencing the growth mode and kinetics[30] that lead to the formation of the core/shell architecture.

The structural characteristics were investigated by 2θ-ω, and pole figure X-ray diffraction scans (XRD; Bruker AXS D8 Advance and Jordan Valley BEDE-D1 diffractometers), respectively. The surface morphologies and nanostructures were studied by scanning electron microscopy (SEM; Carl-Zeiss EVO series), field emission SEM (FE-SEM; Hitachi S5500), transmission electron microscopy (TEM; FEI Technai G^2 S – Twin, operating voltage of 200 kV). High resolution TEM (HR-TEM) and selective area electron diffraction (SAED) were studied using the same TEM apparatus. Low-temperature photoluminescence (PL) spectra were recorded (with 1 m model SPEX 1701 monochromator) using 332 nm He-Cd laser excitation.

3. **Results and discussions**

3.1 Structural properties

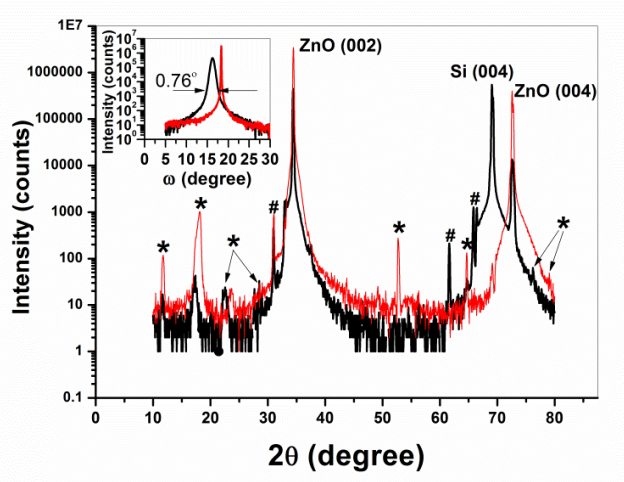

Figure 1. 2θ-ω XRD scans for ZnO/ZnO core/shell nanorods (black line) and a ZnO single crystal wafer (red line) (The features marked '*' are due to the adhesive mounting tape used. The features marked '#' are due to Cu K_β and tungsten L_α radiations from the x-ray tube, the latter

due to contamination). The inset shows the rocking curve scans from the two samples around the ZnO (002) peak position.

Figure 1 shows the 2θ-ω XRD scan, on a log scale, for ZnO/ZnO core/shell nanorods (black line) grown by PLD and similar data from a ZnO single-crystal wafer (red line). The ZnO/ZnO core/shell nanorods show a dominant (002) reflection at $2\theta \approx 34.40^{o}$ and a weaker (004) reflection at $2\theta \approx 72.62^{o}$. The origin of the weaker or impurity features is also mentioned in the figure caption. No other ZnO-related peaks are observable. The intensity of the PLD-deposited ZnO (002) reflection is around a million counts. The ZnO/ZnO core/shell nanorods grown by PLD on Si (100) substrates are clearly highly textured and oriented with their *c*-axes normal to the substrate surface. These data are similar to observations (including the identification of the weaker/impurity peaks) made previously by us and also by others.[31-33] For comparison, we have measured a 2θ-ω XRD scan using *c*-plane terminated ZnO single crystal wafer of thickness 0.5 mm (Tokyo Denpa) using the same conditions (showing red line in Figure 1). The measured 2θ value for the ZnO single crystal (002) reflection is $\approx 34.45^{o}$, identical to the value for our nanorods ($\approx 34.40^{o}$). We have also measured the FWHM of the ZnO (002) reflection for the PLD-deposited ZnO, and used these 2θ and FWHM values to calculate the *c*-axis lattice spacing and crystallite size (more accurately the out-of-plane coherence length), using Bragg's law and the Scherrer equation corrected for instrumental broadening, respectively (we use the weighted average value of the wavelengths of Cu $K\alpha_1$ and Cu $K\alpha_2$ radiation lines for the x-ray wavelength in all calculations, i.e. $\lambda = 1.5425$ Å). The details of the calculation are discussed in a previous article, including correction for the instrumental response when using the Scherrer equation.[34] The PLD-deposited ZnO (002) reflection FWHM, *c*-axis lattice spacing, and crystallite size values are 0.198°, 5.216 Å, and 75.31 nm, respectively. The *c*-axis lattice spacing

value is comparable with the value calculated for the ZnO single crystal wafer (5.207 Å). We note that the value of the lattice spacing (*c*) obtained from the aforementioned single crystal value of 2θ = 34.45º matches precisely the published ZnO *c*-axis lattice spacing of 5.20690 Å (JCPDS card number 36-1451) when rounded off to the third decimal place.

The inset of Figure 1 shows the rocking curve for the (002) reflection from the ZnO/ZnO core/shell nanorods sample (black line) and for the (002) reflection from the ZnO single crystal wafer (red line). The rocking curve of the ZnO/ZnO core/shell nanorods sample has a FWHM of 0.76º which is notably smaller than the data on samples of similar type reported previously for ZnO nanorods.[31,32,35] This, together with the 2θ-ω data, indicates excellent crystallite alignment and texture. We note that, as expected, the FWHM of the rocking curve for the ZnO single crystal wafer is much narrower, essentially limited by the instrument broadening (< 0.1º). Since no catalyst was used as a seed in our synthesis method, no other materials or crystalline phases are identified in the XRD data. In conclusion, the XRD analyses confirm that the ZnO/ZnO core/shell nanorod deposit grown by PLD on Si (100) substrates is well-aligned with excellent *c*-axis orientation normal to the substrate surface.

XRD pole figure analyses were also used to undertake a more detailed investigation of the texture and in-plane orientation of the ZnO/ZnO core/shell nanorods. Pole figures of the (002), (101) and (102) planes were measured at 2θ values of 34.5°, 36.5° and 47.5°, respectively (Figure 2). Figure 2 (a) shows a narrow and intense (002) pole figure centered at Ψ=0 indicating the growth of the core/shell nanorods with their vertical axes along the substrate normal. Figures 2 (b) and (c) show rotationally (circularly) symmetric (101) and (102) pole figures at Ψ angle values of ~ 62.7° and ~ 42.9°, respectively. The latter are very close to the value of the angles between the ZnO (101)/(002) and (102)/(002) planes, as expected from the known

crystallographic structure of ZnO.[36,37] The intense spots at Ψ = 45° on the (102) pole figure, indicated in Figure 2 (c), are due to the (220) planes of the Si substrate, and seen previously.[36] The pole figure data confirm that the PLD grown ZnO/ZnO core/shell nanorods are well textured with excellent vertical orientation along the *c*-axis and also show the complete absence of any in-plane orientation, i.e. the absence of epitaxy, on the substrate.

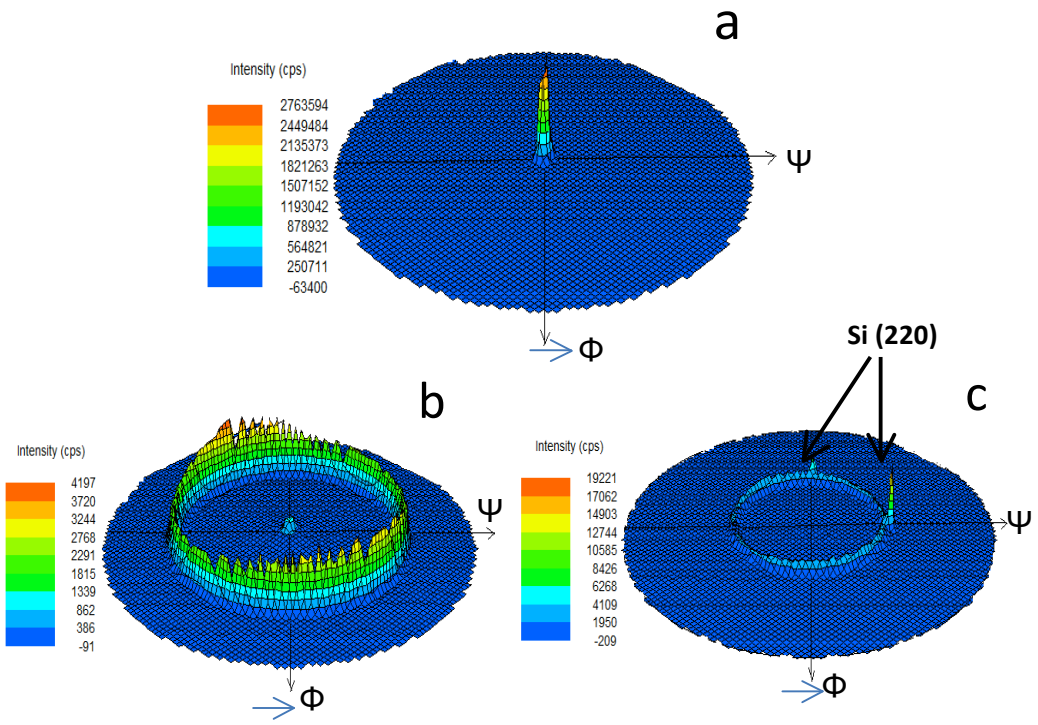

Figure 2. XRD pole figures for the (a) (002), (b) (101) and (c) (102) ZnO planes, respectively, in ZnO/ZnO core/shell nanorods grown by PLD.

3.2 Surface morphology and nanostructuring

The surface morphologies of the core/shell nanorod deposits were studied using SEM, FE-SEM, and TEM. Figures 3(a), (b) and (d) show FE-SEM images, and Figure 3(c) shows SEM images, taken at various tilt angles. These images show that the core/shell nanorods have almost

conical terminations with rounded or blunt tips. Figure 3 also strongly supports the conclusions from XRD (2θ-ω and X-ray pole figures) analysis concerning preferred *c*-axis orientation and the absence of in-plane epitaxial ordering. The SEM and FE-SEM images of Figure 3 allow us to conclude that the core/shell nanorods are densely packed, with a uniform morphology.

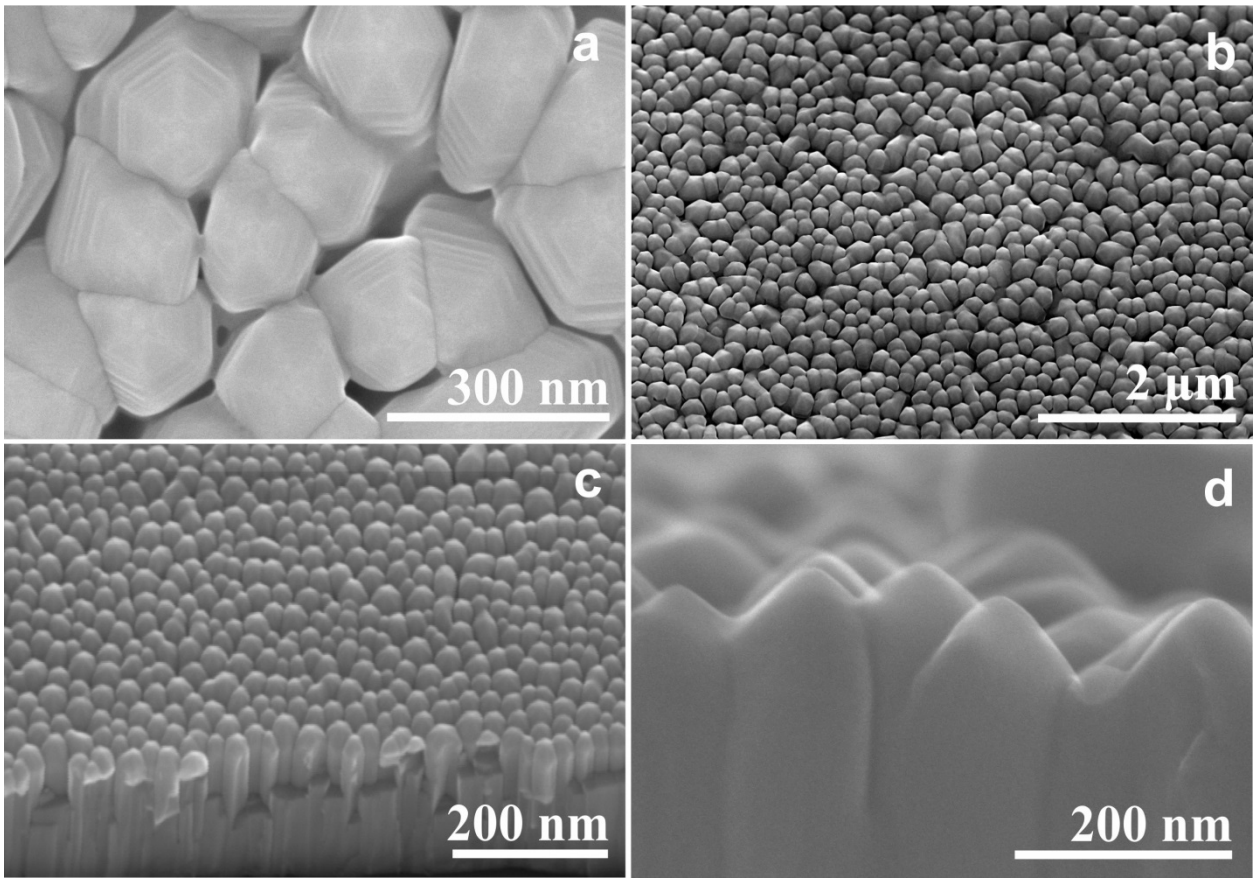

Figure 3. Field emission SEM (a), (b) and (d) and SEM (c) images of ZnO/ZnO core/shell nanorods grown by PLD at (a) 0º tilt (plane view), (b) 20º tilt, (c) 30º tilt, and (d) 85º tilt angles.

Significant insights into the core/shell nanorods structure were revealed using TEM and HR-TEM analyses, as discussed below. Regions of the samples containing hundreds of ZnO/ZnO core/shell nanorods were peeled off the Si (100) substrate using a surgical blade and mounted on the 300 mesh size TEM grid for analysis. Figure 4, (c), (d) shows TEM ((a)) and

HR-TEM ((b), (c) and (d)) images of the core/shell nanorods, respectively. The images in Figures 4 (a) and (b) show that the nanorods have a core/shell structure with a crystalline (cr) core and an amorphous (am) shell. We now use the "cr-ZnO/am-ZnO core/shell" terminology to accurately refer to the established structure of the nanorods. Further detailed investigations were made at different locations of a specific core/shell nanorod, indicated by the circled regions marked 'b, c and d' in Figure 4(a), corresponding to the images shown in Figure 4 (b), (c) and (d). The inset of Figure 4 (b) shows a HR-TEM image at the core/shell boundary region of the cr-ZnO/am-ZnO core/shell nanorods. These data confirm in greater detail the core/shell structure. An artificial line was drawn as a guide to the eye in Figure 4 (b) to show the crystalline core and amorphous shell regions. The cr-core/am-shell structure can be at least partially explained by the combination of several plausible factors such as the rate of material deposition prevailing in the PLD apparatus at the 800 °C substrate temperature, shadowing effects due the compact nanorod distribution and the final cooling rate. All of these factors may contribute to prevent the adatom diffusion necessary to find an equilibrium lattice site in the crystalline growth directions perpendicular to the c-axis. Additionally, we note that such cr-core/am-shell structures have also been produced serendipitously in previous works using different growth methods.[17,19-21,24]

The HR-TEM image of the core part of the core/shell nanorods (indicated by circled region c in Figure 4(a)) is represented in Figure 4 (c) and the observed lattice spacing from HR-TEM (0.27 nm) is in good agreement with that obtained from the XRD data above (0.26 nm). The selected area electron diffraction (SAED) pattern was collected using a 200 nm aperture and is shown in the inset of Figure 4 (c). The ring pattern in SAED indicates the field of view contains polycrystalline material. The indexed (002), (101), (102) and (110) diffraction peaks belong to

the pure ZnO phase and provide information complementary to the XRD pole figure data above. The HR-TEM data also allows us to identify specific regions at the interface between the crystalline core and amorphous shell, indicated by the round circles (from the circled region d of Figure 4 (a)) in Figures 4 (d) which display clear evidence of Moiré fringes at the boundary. Li et al. identified no Moiré patterns in their HR-TEM data from PLD grown ZnO/Er_2O_3 core/shell nanorods, because their Er_2O_3 shell region was polycrystalline.[8] Overall, the TEM and HR-TEM data clearly shows that cr-ZnO/am-ZnO core/shell nanorods grown by PLD on Si (100) substrates have a core/shell structure (with a crystalline core and an amorphous shell) with Moiré fringes identified at the boundary region where structural defects are expected, which may well be associated with the core/shell boundary interface region.

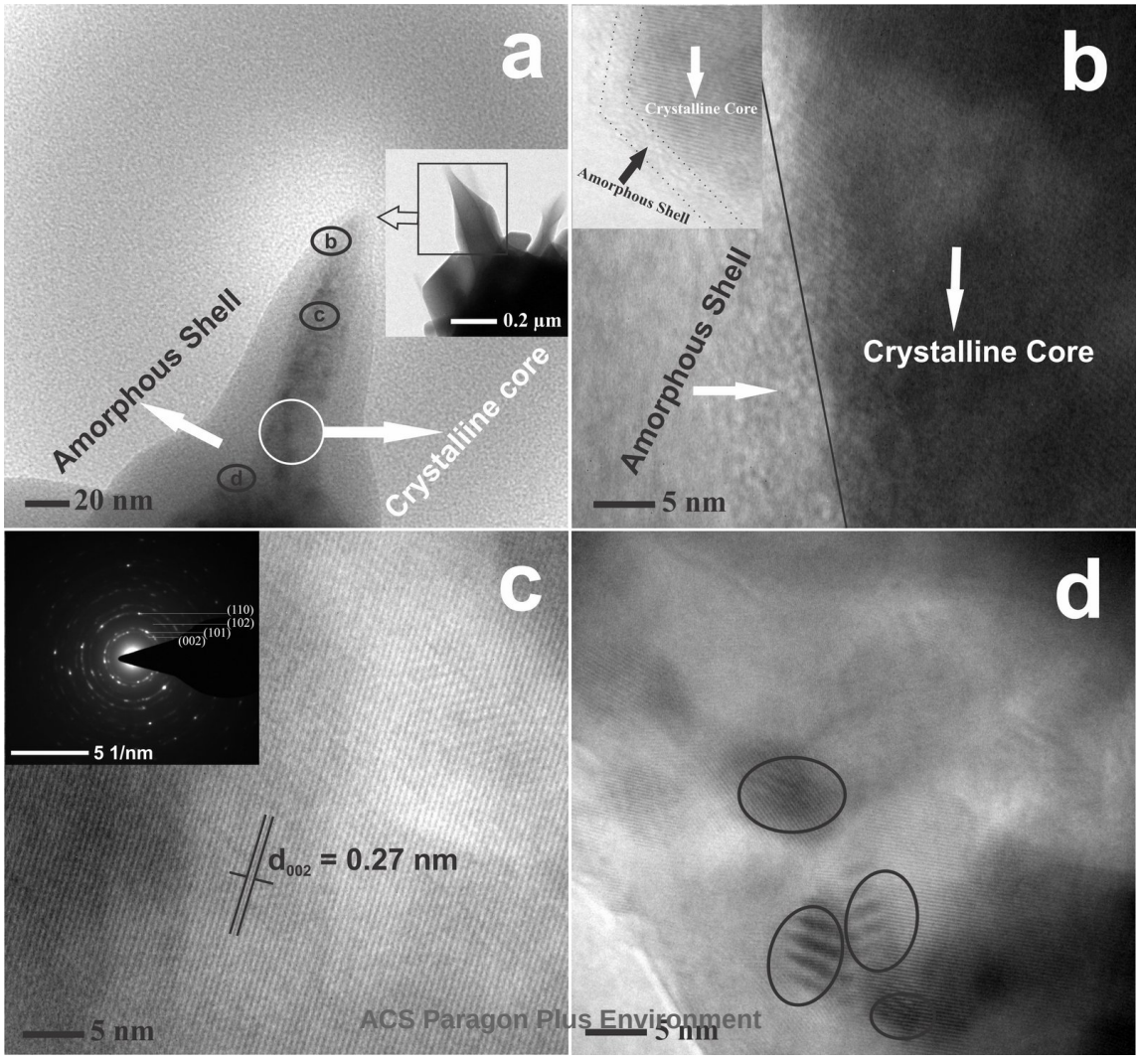

Figure 4. TEM, HR-TEM and SAED images of cr-ZnO/am-ZnO core/shell nanorods grown by PLD; (a): TEM image of a core/shell nanorod; (b): crystalline core and amorphous shell boundary region of a nanorod in the area indicated by circle b in (a); (c): HR-TEM image for the core-part of a core/shell nanorod in the area indicated by circle c in (a); (d): Identified Moiré fringes in the area indicated by circle d in (a). Inset of (c) shows SAED pattern of the area shown in (c).

3.3 Optical Properties

Because of intrinsic and extrinsic defects/impurities, which lead to a range of donor/acceptor levels within the bandgap, ZnO can emit right across the visible spectrum, as well as in the near UV.[38,39] This is a key advantage for devices such as white light LEDs. However, the absence of stable and high hole mobility p-type material[40] remains the major obstacle for the development of large scale LEDs and laser diodes, and this, in turn, is due to the nature of the defect population in the material itself. In this regard, it remains of crucial importance to understand the defect population in this material, and a powerful tool for the study of such defects is their photoluminescence emission.

Figure 5 shows a typical low-temperature (13 K) PL spectrum of the cr-ZnO/am-ZnO core/shell nanorods produced in this work. Figure 5 (a) reveals a strong I_6 line at 3.36 eV, which is generally attributed due to Al impurities, as well as a surface exciton (labelled SE) at 3.366 eV, and free exciton emission (labelled FE) at 3.377 eV (A_L: longitudinal free exciton-polariton)

and 3.373 eV (A_T: transverse free exciton-polariton). Interestingly, an additional broad emission at 3.331 eV was also consistently observed in the low-temperature PL spectra of these samples. Defect-related emissions at 3.31 eV, 3.3328 eV, 3.3363 eV, 3.333 eV and 3.3465 eV have been observed in various ZnO structures including bulk, single crystals, micro-/nano-crystals, heterostructures, quantum dots, 1D structures (nanorods and nanowires) and also in p-type ZnO.[41-46] However, the present work identifies a new defect emission at 3.331 eV in these cr-ZnO/am-ZnO core/shell nanorods grown on ZnO buffer layers/Si (100) substrates by PLD. In a number of cases the emissions listed above have been associated with structural defects in ZnO crystals.[41,42,44] We note that, in previous articles, the emission lines observed at 3.3328 eV and 3.3363 eV in a ZnO single crystals are labeled as Y_0 and Y_1, respectively,[42] Furthermore the feature at 3.3328 eV (Y_0) is also labeled in some publications as a DBX (donor bound exciton),[47] and as a DD (deep donor bound exciton), emission.[43,48] The emission at 3.331 eV observed in this work is considerably broader (FWHM ~1.75 meV) than the emissions observed in these other works (FWHM~ 0.5 meV and 0.2 meV),[41,42] as well as displaying a clearly asymmetric line shape. Deep level visible emission was also observed from the cr-ZnO/am-ZnO core/shell nanorods, as shown in Figure 5 (b) where the structured green band, due to Cu impurities, is clearly observed.[49]

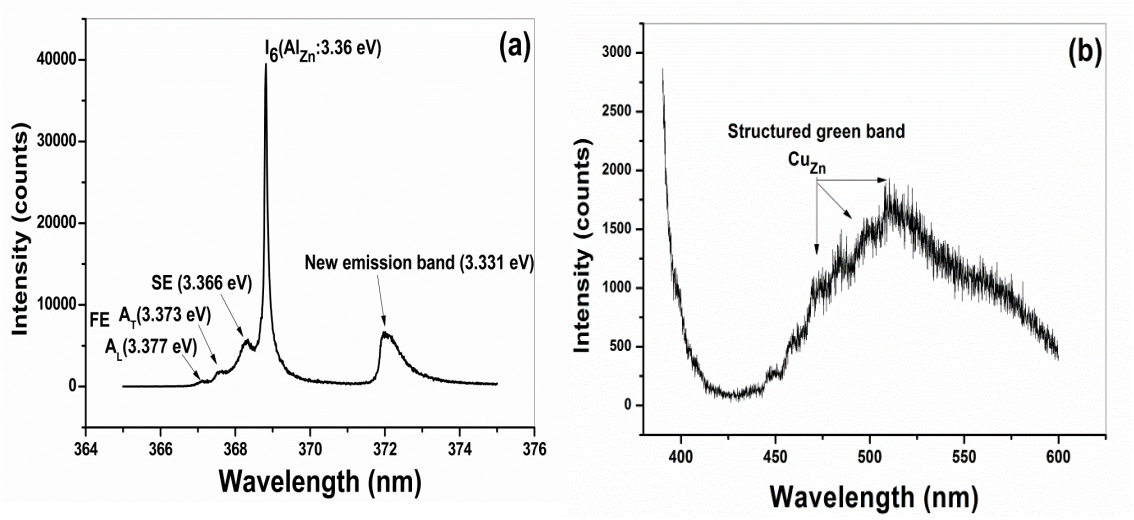

Figure 5. Low temperature (13 K) PL spectra of cr-ZnO/am-ZnO core/shell nanorods (a) near band-edge region showing new emission band at 3.331 eV and (b) visible region showing structured green band emission.

The 3.331 eV emission was further investigated by varying temperature and laser excitation power. Figure 6 (a) shows temperature dependent PL spectra from 13 K to 100 K. We observed that as temperature increases the surface and shallow bound exciton emissions quench rapidly. It is clear that the initially strong I_6 line reduces in intensity much faster compared to the 3.331 eV band. The 3.331 eV band can still be clearly seen at a temperature of 100 K and this behavior implies involvement of deeply bound constituents, either an electron or a hole or both. Generally, two electron satellite (TES) and longitudinal optical (LO) replicas of the line are located in a region 30 - 70 meV from the parent emissions. However, since the 3.331 eV band still remains visible at a temperature (100 K) where the shallow bound exciton emission has been quenched, it is not due to a TES of the shallow bound exciton emission. We note that TES of the dominant I_6 line and TES and an LO replica of the 3.331 eV emission are also observed in Figure 6 (a). These temperature dependent PL studies enable us to conclude that the 3.331 eV emission is stable up to 100 K and therefore it is neither a shallow bound exciton, nor a TES or phonon replica of a shallower bound exciton transition, and is therefore the zero phonon line associated with the recombination of deeply bound carriers at a defect in the material.

We have also varied the laser excitation power (using neutral density filters), at a fixed cryostat temperature of 13 K, as shown in Figure 6(b). The 3.331 eV band remains visible and its

shape largely unchanged with varying power of the laser. Slight laser heating effects can just be distinguished at the highest laser power of 6.90 mW, where a small redshift in emission is seen across the entire near band-edge region. It is however clearly observed in Figure 6(c) that the 3.331 eV band scales in a similar manner to the I_6 shallow bound exciton emission with varying laser excitation power, even at the highest laser powers. This clearly demonstrates that the 3.331 eV emission is associated with a single electron-hole recombination, rather than a bi-exciton or other multi-electron-hole pair crystal excitation, and the slight effects of laser heating at the highest laser power do not in any way affect this conclusion.

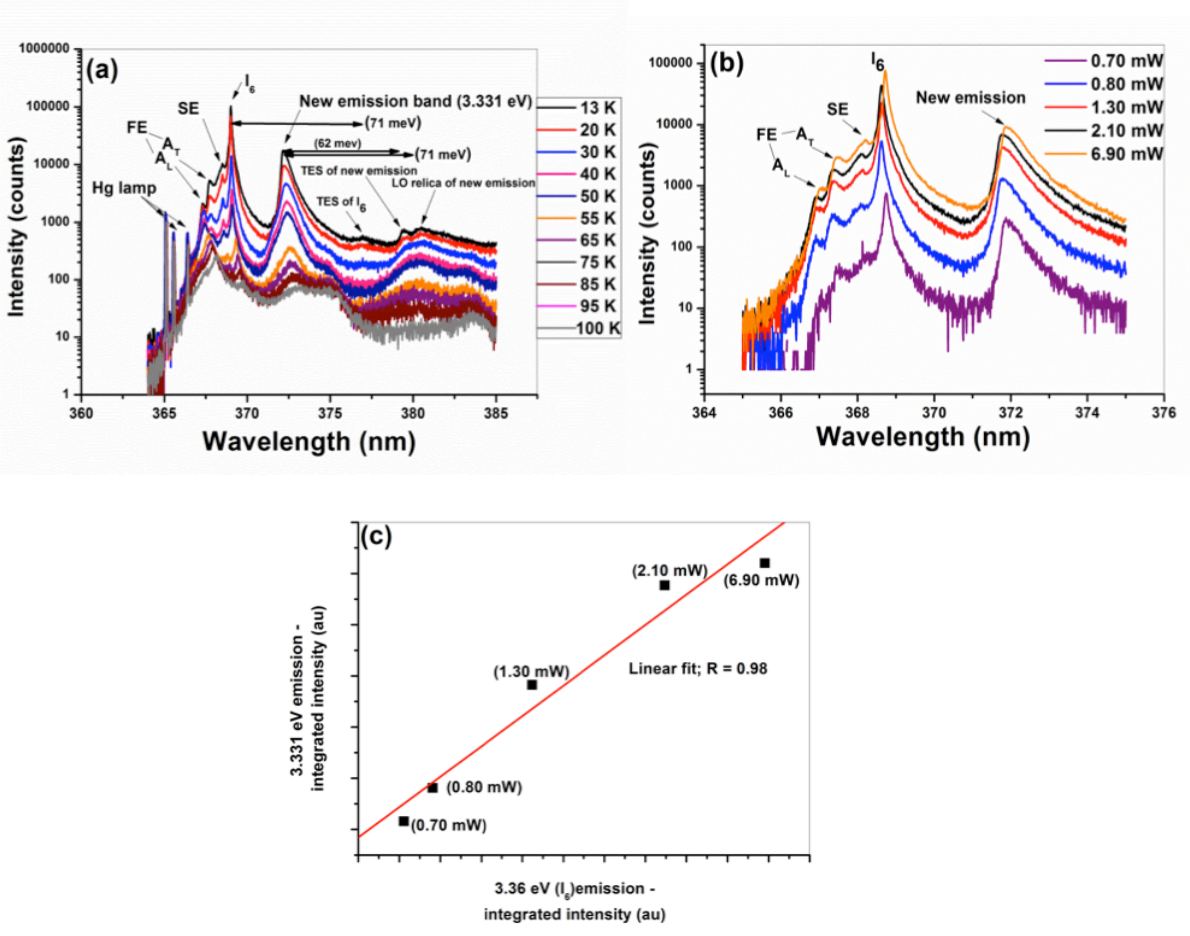

Figure 6. (a) Dependence of PL emission from cr-ZnO/am-ZnO core/shell nanorods on temperature, (b) Dependence of PL emission from cr-ZnO/am-ZnO core/shell nanorods on laser excitation power at constant temperature of 13 K and (c) Linear correlation between the integrated intensities of the I_6 (3.36 eV) and 3.331 eV emission bands for the various laser powers used in this work.

Based on the similarity in emission energy of the 3.331 eV band to that seen for other structural defect-related UV emissions,[41,42,44] and the simultaneous presence of structural defects at the boundary region of our core/shell nanorods, as revealed by HR-TEM data above (Figure 4 (d)), we propose that the origin of the 3.331 eV band is electron-hole recombination at structural defects associated with the core/shell boundary interface region. This assignment is based on: (i) the demonstrated presence of structural defects at the boundary region of the core/shell nanorods, as shown by HR-TEM, in samples which exhibit this 3.331 eV band emission, (ii) the deeper spectral position of the emission, similar to PL emissions from other structural defects in ZnO, which is also consistent with the temperature stability of the emission, and (iii) the expected presence of structural defects with slightly different environments at the core/shell boundary region which explains the relatively large line-width of the 3.331 eV emissions, since the slightly differing structural defect environments give rise to slight changes in emission energy from individual defects, and the ensemble effect yields the broader emission band observed in measurements.

Conclusions

We have grown, for the first time, self-organized cr-ZnO/am-ZnO core/shell nanorods on Si (100) wafers by PLD, without using a metal catalyst seed and without the need for a separate

growth stage for the shell region. This was achieved by using a specific sequence of heating and cooling phases pre- and post-deposition. The deposits were characterized using x-ray diffraction, electron microscopies and photoluminescence. The characterization studies showed that the nanorods are highly textured with their *c*-axis oriented normal to, but without epitaxial in-plane ordering on, the substrate surface. The nanorods have conical terminations with rounded/blunt tips. They present unique core/shell architecture with a crystalline core and an amorphous shell while structural defects feature in the region of the core/shell boundary interface. The samples exhibit a previously unreported emission band at 3.331 eV in their low-temperature photoluminescence spectrum. This emission arises from a single electron-hole pair recombination involving deeply bound constituents likely associated with the structural defects at the core/shell boundary interface region.

The unique architecture and properties of the core/shell cr-ZnO/am-ZnO nanorods produced in this work should prove useful in applications where the functionality arises from the presence of an amorphous shell on a ZnO crystalline nanorod core. Examples of such applications would be in ZnO supercapacitor electrodes for energy storage, the passivation of ZnO photoanodes in dye-sensitized solar cells or the control of the emission properties of ZnO nanolasers.

AUTHOR INFORMATION

Corresponding Author: Dr. Jean-Paul Mosnier

Email: jean-paul.mosnier@dcu.ie, Tel: +353-17005303.

AUTHOR CONTRIBUTIONS

The manuscript was written through contributions of all authors. All authors have given approval to the final version of the manuscript.

ACKNOWLEDGMENTS

Mr Saikumar Inguva acknowledges the award of a postgraduate studentship from "INSPIRE (Integrated Nanoscience Platform for Ireland)". This INSPIRE-funded work was conducted under the framework of the Irish Government's Programme for Research in Third Level Institutions Cycle 5, National Development Plan 2007-2013 with the assistance of the European Regional Development Fund. The authors also gratefully acknowledge Mr. Ciarán Gray and Dr Joseph Cullen for their assistance with the low-temperature PL experiments, as well as Dr Brendan Twamley for his help with the FE-SEM measurements.

ABBREVIATIONS

ZnO, zinc oxide; PLD, pulsed laser deposition; mT, millitorr; FWHM, full width half maximum; XRD, X-ray diffraction; PL, photoluminescence; FE-SEM, field emission scattering electron microscopy; TEM, transmission electron microscopy; HR-TEM, high resolution transmission electron microscopy; SAED, selected area electron diffraction; LO, longitudinal optical; TES, two electron satellite; DBX, donor bound exciton; DD, Deep donor bound exciton.

References

(1) Lee, C.; Chen, D. Large-scale synthesis of Ni-Ag core-shell nanoparticles with magnetic, optical and anti-oxidation properties. *Nanotechnology* **2006**, *17*, 3094-3099.

(2) Zhu, Y. F.; Fan, A. H.; Shen, W. Z. A general chemical conversion route to synthesize various ZnO-based core/shell structures. J. Phys. Chem. C **2008**, *112*, 10402-10406.

(3) Panda, S. K.; Dev, A.; Chaudhuri, S. Fabrication and luminescent properties of c-axis oriented ZnO-ZnS core-shell and ZnS nanorod arrays by sulfidation of aligned ZnO nanorod arrays. J. Phys. Chem. C **2007**, *111*, 5039-5043.

(4) Gao, T.; Li, Q.; Wang, T. Sonochemical synthesis, optical properties, and electrical properties of core/shell-type ZnO nanorod/CdS nanoparticle composites. *Chem. Mater.* **2005**, *17*, 887-892.

(5) Lin, Y.; Hung, Y.; Lin, H.; Tseng, Y.; Chen, Y.; Mou, C. Photonic crystals from monodisperse lanthanide-hydroxide-at-silica core/shell colloidal spheres. *Adv. Mater.* **2007**, *19*, 577–580.

(6) Jang, J.; Nam, Y.; Yoon, H. Fabrication of polypyrrole-poly(n-vinylcarbazole) core-shell nanoparticles with excellent electrical and optical properties. *Adv. Mater.* **2005**, *17*, 1382-1386.

(7) Caruso, F. Nanoengineering of particle surfaces. *Adv. Mater.* **2001**, *13*, 11-22.

(8) Li, S. Z.; Gan, C. L.; Cai, H.; Yuan, C. L.; Guo, J.; Lee, P. S.; Ma, J. Enhanced photoluminescence of ZnO/Er_2O_3 core-shell structure nanorods synthesized by pulsed laser deposition. *Appl. Phys. Lett.* **2007**, *90*, 263106.

(9) Wang, Z. L. Novel nanostructures of ZnO for nanoscale photonics, optoelectronics, piezoelectricity, and sensing. *Appl.Phys. A: Mater. Sci. Process.* **2007**, *88*, 7-15.

(10) Wang, Z.; Song, J. Piezoelectric nanogenerators based on zinc oxide nanowire arrays. *Science* **2006**, *312*, 242-246.

(11) Liu, Y.; Zhong, M.; Shan, G.; Li, Y.; Huang, B.; Yang, G. Biocompatible ZnO/Au nanocomposites for ultrasensitive DNA detection using resonance Raman scattering. *J. Phys. Chem. B* **2008**, *112*, 6484-6489.

(12) Si, S.; Li, C.; Wang, X.; Peng, Q.; Li, Y. Fe_2O_3/ZnO core-shell nanorods for gas sensors. *Sensors Actuators B* **2006**, *119*, 52-56.

(13) Huang, B.; Lin, J. Core-shell structure of zinc oxide/indium oxide nanorod based hydrogen sensors. *Sensors Actuators B* **2012**, *174*, 389-393.

(14) Schrier, J.; Demchenko, D. O.; Wang, L. Optical properties of ZnO/ZnS and ZnO/ZnTe heterostructures for photovoltaic applications. *Nano Lett.* **2007**, *7*, 2377-2382.

(15) Greene, L. E.; Law, M.; Yuhas, B. D.; Yang, P. ZnO-TiO_2 core-shell nanorod/P3HT solar cells. *J. Phys. Chem. C* **2007**, *111*, 18451-18456.

(16) Kanmani, S. S.; Ramachandran, K. Synthesis and characterization of TiO_2/ZnO core/shell nanomaterials for solar cell applications. *Renewable Energy* **2012**, *43*, 149-156.

(17) Wang, M.; Huang, C.; Cao, Y.; Yu, Q.; Guo, W.; Huang, Q.; Liu, Y.; Huang, Z.; Huang, J.; Wang, H.; Deng, Z. The effects of shell characteristics on the current-voltage behaviors of dye-sensitized solar cells based on ZnO/TiO_2 core/shell arrays. *Appl. Phys. Lett.* **2009**, *94*, 263506.

(18) Li, G.; Wang, Z.; Zheng, F.; Ou, Y.; Tong, Y. ZnO@MoO_3 core/shell nanocables: facile electrochemical synthesis and enhanced supercapacitor performances. *J. Mater. Chem.* **2011**, *21*, 4217-4221.

(19) Yang, P.; Xiao, X.; Li, Y.; Ding, Y.; Qiang, P.; Tan, X.; Mai, W.; Lin, Z.; Wu, W.; Li, T.; Jin, H.; Liu, P.; Zhou, J.; Wong, C. P.; Wang, Z. L. Hydrogenated ZnO Core-Shell Nanocables for Flexible Supercapacitors and Self-Powered Systems. *ACS Nano* **2013**, *7*, 2617-2626.

(20) Xia, X.; Tu, J.; Zhang, Y.; Wang, X.; Gu, C.; Zhao, X.; Fan, H. J. High-Quality Metal Oxide Core/Shell Nanowire Arrays on Conductive Substrates for Electrochemical Energy Storage. *ACS Nano* **2012**, *6*, 5531-5538.

(21) Wang, Z.; Guo, R.; Li, G.; Ding, L.; Ou, Y.; Tong, Y. Controllable synthesis of ZnO-based core/shell nanorods and core/shell nanotubes. *RSC Adv.* **2011**, *1*, 48-51.

(22) Trejo, M.; Santiago, P.; Sobral, H.; Rendon, L.; Pal, U. Synthesis and Growth Mechanism of One-Dimensional Zn/ZnO Core-Shell Nanostructures in Low-Temperature Hydrothermal Process. *Cryst. Growth Des.* **2009**, *9*, 3024-3030.

(23) Zeng, H.; Cai, W.; Cao, B.; Hu, J.; Li, Y.; Liu, P. Surface optical phonon Raman scattering in Zn/ZnO core-shell structured nanoparticles. *Appl. Phys. Lett.* **2006**, *88*, 181905.

(24) Zhou, H.; Alves, H.; Hofmann, D.; Kriegseis, W.; Meyer, B.; Kaczmarczyk, G.; Hoffmann, A. Behind the weak excitonic emission of ZnO quantum dots: ZnO/$Zn(OH)_2$ core-shell structure. *Appl. Phys. Lett.* **2002**, *80*, 210-212.

(25) Kaydashev, V. E.; Kaidashev, E. M.; Peres, M.; Monteiro, T.; Correia, M. R.; Sobolev, N. A.; Alves, L. C.; Franco, N.; Alves, E. Structural and optical properties of $Zn_{0.9}Mn_{0.1}O$/ZnO core-shell nanowires designed by pulsed laser deposition. *J. Appl. Phys.* **2009**, *106*, 093501.

(26) Mosnier, J. P.; O'Haire, R. J.; McGlynn, E.; Henry, M. O.; McDonnell, S. J.; Boyle, M. A.; McGuigan, K. G. ZnO films grown by pulsed-laser deposition on soda lime glass substrates for the ultraviolet inactivation of Staphylococcus epidermidis biofilms. *Sci. Technol. Adv. Mater.* **2009**, *10*, 045003.

(27) Klingshirn, C. F.; Meyer, B. K.; Waag, A.; Hoffmann, A.; Geurts, J. In *Zinc Oxide-From Fundamental Properties Towards Novel Applications;* Hull, R., Jagadish, C., Osgood, R. M., Parisi, J., Wang, Z.;Warlimount, H., Eds.; Springer: Berlin, 2010; *120*, Chapter-3, pp 66-67.

(28) Tien, L. C.; Pearton, S. J.; Norton, D. P.; Ren, F. Synthesis and microstructure of vertically aligned ZnO nanowires grown by high-pressure-assisted pulsed-laser deposition. *J. Mater. Sci.* **2008**, *43*, 6925–6932.

(29) Willander, M.; Nur, O.; Zhao, Q. X.; Yang, L. L.; Lorenz, M.; Cao, B. Q.; Perez, J. Z.; Czekalla, C.; Zimmermann, G.; Grundmann, M.; Bakin, A.; Behrends, A.; Al-Suleiman, M.; El-Shaer, A.; Mofor, A. C.; Postels, B.; Waag, A.; Boukos, N.; Travlos, A.; Kwack, H. S.; Guinard, J.; Dang, D. L. S. Zinc oxide nanorod based photonic devices: recent progress in growth, light emitting diodes and lasers. *Nanotechnology* **2009**, *20*, 332001.

(30) Eason, R., Ed.; In *Pulsed Laser Deposition of Thin films: Applications-Led Growth of Functional Materials;* Wiley: Hoboken, NJ, 2007; Chapter 8, p 177-180 and Chapter 12, p 268-282.

(31) Kumar, R. T. R.; McGlynn, E.; McLoughlin, C.; Chakrabarti, S.; Smith, R. C.; Carey, J. D.; Mosnier, J. P.; Henry, M. O. Control of ZnO nanorod array density by Zn supersaturation variation and effects on field emission. *Nanotechnology* **2007**, *18*, 215704.

(32) McCarthy, E.; Kumar, R. T. R.; Doggett, B.; Chakrabarti, S.; O'Haire, R. J.; Newcomb, S. B.; Mosnier, J. P; Henry, M. O.; McGlynn, E. Effects of the crystallite mosaic spread on integrated peak intensities in 2 theta-omega measurements of highly crystallographically textured ZnO thin films. *J. Phys. D: Appl. Phys.* **2011**, *44*, 375401.

(33) Wan, W.; Zhu, L.; Hu, L.; Chen, G.; Mi, W.; Ye, Z. Investigation of morphology evolution of Cu-ZnO nanorod arrays and enhancement of ferromagnetism by codoping with N. *Phys. Lett. A* **2014**, *378*, 2763-2767.

(34) Mote, V. D.; Purushotham, Y.; Dole, B. N. Williamson-Hall Analysis in Estimation of Laticce Strain in Nanometer-Sized ZnO Particles. *J. Theor. Appl. Phys.* **2012**, *6*, 1-8.

(35) Jie, J.; Wang, G.; Chen, Y.; Han, X.; Wang, Q.; Xu, B.; Hou, J. Synthesis and optical properties of well-aligned ZnO nanorod array on an undoped ZnO film. *Appl. Phys. Lett.* **2005**, *86*, 031909.

(36) Teki, R.; Parker, T. C.; Li, H.; Koratkar, N.; Lu, T.; Lee, S. Low temperature synthesis of single crystalline ZnO nanorods by oblique angle deposition. *Thin Solid Films* **2008**, *516*, 4993-4996.

(37) Morkoç, H.; Özgür, Ü. In *Zinc Oxide-Fundamentals, Materials and Device Technology;* Wiley-VCH: Germany, 2009; Chapter-1 and 2.

(38) Djurisic, A.; Leung, Y.; Tam, K.; Ding, L.; Ge, W.; Chen, H.; Gwo, S. Green, yellow, and orange defect emission from ZnO nanostructures: Influence of excitation wavelength. *Appl. Phys. Lett.* **2006**, *88*, 103107.

(39) Liu, W.; Gu, S.; Ye, J.; Zhu, S.; Liu, S.; Zhou, X.; Zhang, R.; Shi, Y.; Zheng, Y.; Hang, Y.; Zhang, C. Blue-yellow ZnO homostructural light-emitting diode realized by metalorganic chemical vapor deposition technique. *Appl. Phys. Lett.* **2006**, *88*, 092101.

(40) Look, D.C.; Claflin, B.; Alivov, Y.; Park, S. The future of ZnO light emitters. *phys. stat. sol. A* **2004**, *201*, 2203-2212.

(41) Schirra, M.; Schneider, R.; Reiser, A.; Prinz, G. M.; Feneberg, M.; Biskupek, J.; Kaiser, U.; Krill, C. E.; Thonke, K.; Sauer, R. Stacking fault related 3.31-eV luminescence at 130-meV acceptors in zinc oxide. *Phys. Rev. B* **2008**, *77*, 125215.

(42) Wagner, M. R.; Callsen, G.; Reparaz, J. S.; Schulze, J. -.; Kirste, R.; Cobet, M.; Ostapenko, I. A.; Rodt, S.; Nenstiel, C.; Kaiser, M.; Hoffmann, A.; Rodina, A. V.; Phillips, M. R.; Lautenschlaeger, S.; Eisermann, S.; Meyer, B. K. Bound excitons in ZnO: Structural defect complexes versus shallow impurity centers. *Phys. Rev. B* **2011**, *84*, 035313.

(43) Johnston, K.; Henry, M.; McCabe, D.; McGlynn, E.; Dietrich, M.; Alves, E.; Xia, M. Identification of donor-related impurities in ZnO using photoluminescence and radiotracer techniques. *Phys. Rev. B* **2006**, *73*, 165212.

(44) Alves, H.; Pfisterer, D.; Zeuner, A.; Riemann, T.; Christen, J.; Hofmann, D.; Meyer, B. Optical investigations on excitons bound to impurities and dislocations in ZnO. *Opt. Mater.* **2003**, *23*, 33-37.

(45) Reynolds, J. G.; Reynolds, C. L., Jr.; Mohanta, A.; Muth, J. F.; Rowe, J. E.; Everitt, H. O.; Aspnes, D. E. Shallow acceptor complexes in p-type ZnO. *Appl. Phys. Lett.* **2013**, *102*, 152114.

(46) Lange, M.; Zippel, J.; Benndorf, G.; Czekalla, C.; Hochmuth, H.; Lorenz, M.; Grundmann, M. Temperature dependence of localization effects of excitons in ZnO/$Cd_xZn_{1-x}O$/ZnO double heterostructures. *J. Vac. Sci. Technol. B* **2009**, *27*, 1741-1745.

(47) Meyer, B.; Alves, H.; Hofmann, D.; Kriegseis, W.; Forster, D.; Bertram, F.; Christen, J.; Hoffmann, A.; Strassburg, M.; Dworzak, M.; Haboeck, U.; Rodina, A. Bound exciton and donor-acceptor pair recombinations in ZnO. *phys. stat. sol. B* **2004**, *241*, 231-260.

(48) Schildknecht, A.; Sauer, R.; Thonke, K. Donor-related defect states in ZnO substrate material. *Physica B:Condens.Matter*. **2003**, *340*, 205-209.

(49) Byrne, D.; Herklotz, F.; Henry, M. O.; McGlynn, E. Unambiguous identification of the role of a single Cu atom in the ZnO structured green band. *J. Phys.:Condens. Matter*. **2012**, *24*, 215802.

Table of Contents (TOC)

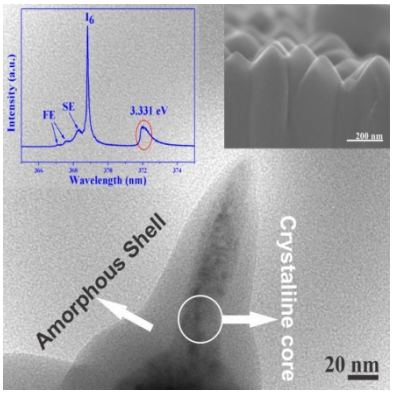

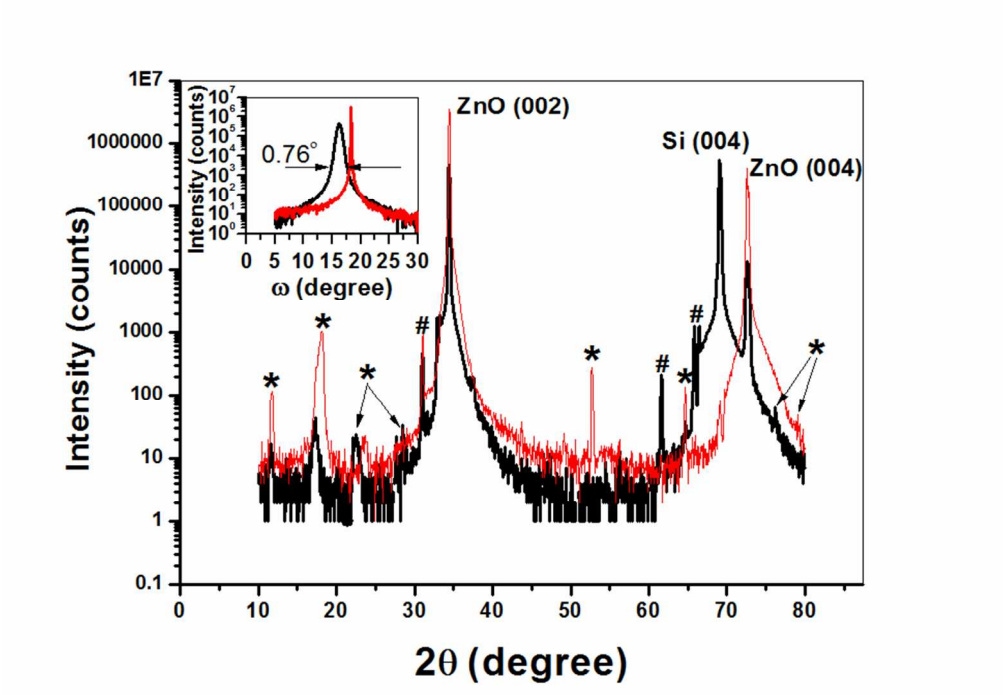

2θ-ω XRD scans for ZnO-ZnO core-shell nanorods (black line) and a ZnO single crystal wafer (red line) (The features marked '*' are due to the adhesive mounting tape used. The features marked '#' are due to Cu Kβ and tungsten Lα radiations from the x-ray tube, the latter due to contamination). The inset shows the rocking curve scans from the two samples around the ZnO (002) peak position.
81x57mm (300 x 300 DPI)

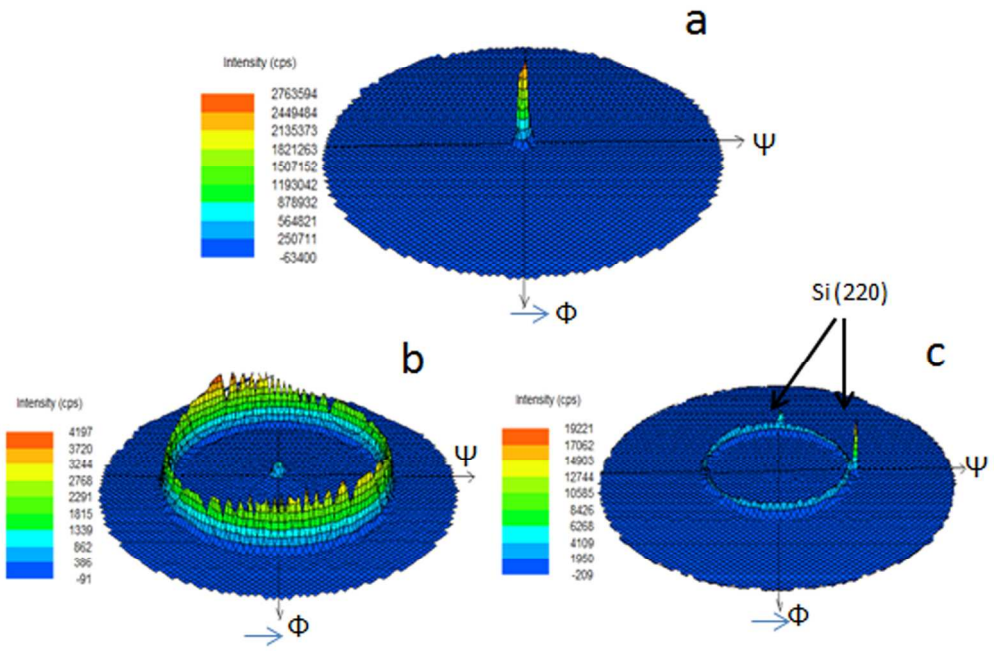

XRD pole figures for the (a) (002), (b) (101) and (c) (102) ZnO planes, respectively, in ZnO-ZnO core-shell nanorods grown by PLD.
196x134mm (300 x 300 DPI)

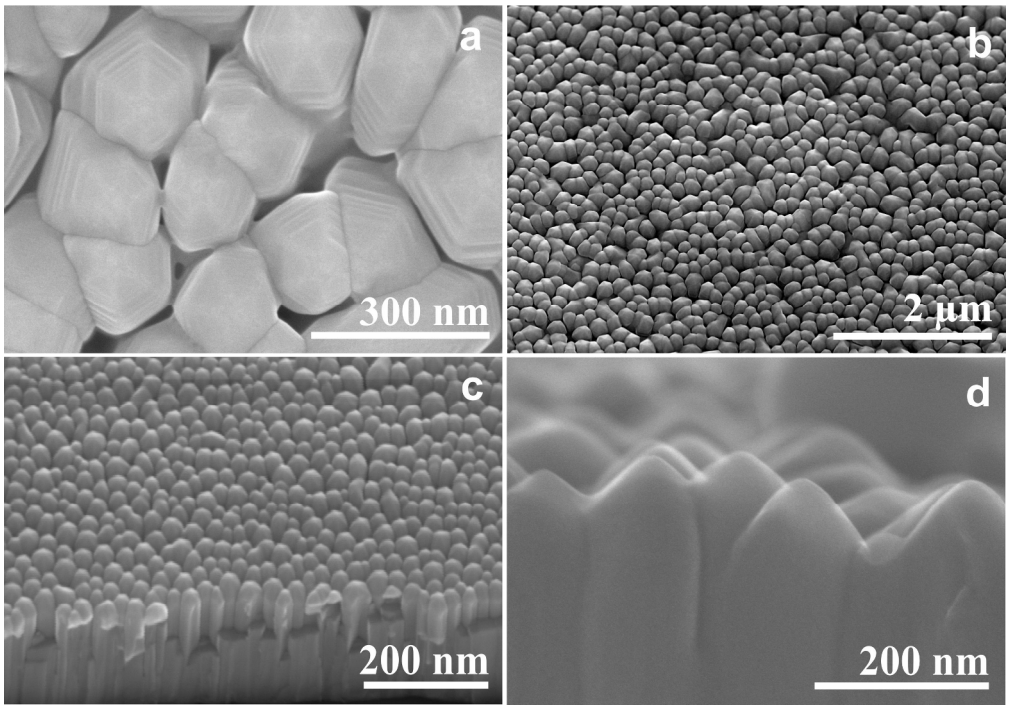

Field emission SEM (a), (b) and (d) and SEM (c) images of ZnO-ZnO core-shell nanorods grown by PLD at (a) 0º tilt (plane view), (b) 20º tilt, (c) 30º tilt, and (d) 85º tilt angles
255x178mm (300 x 300 DPI)

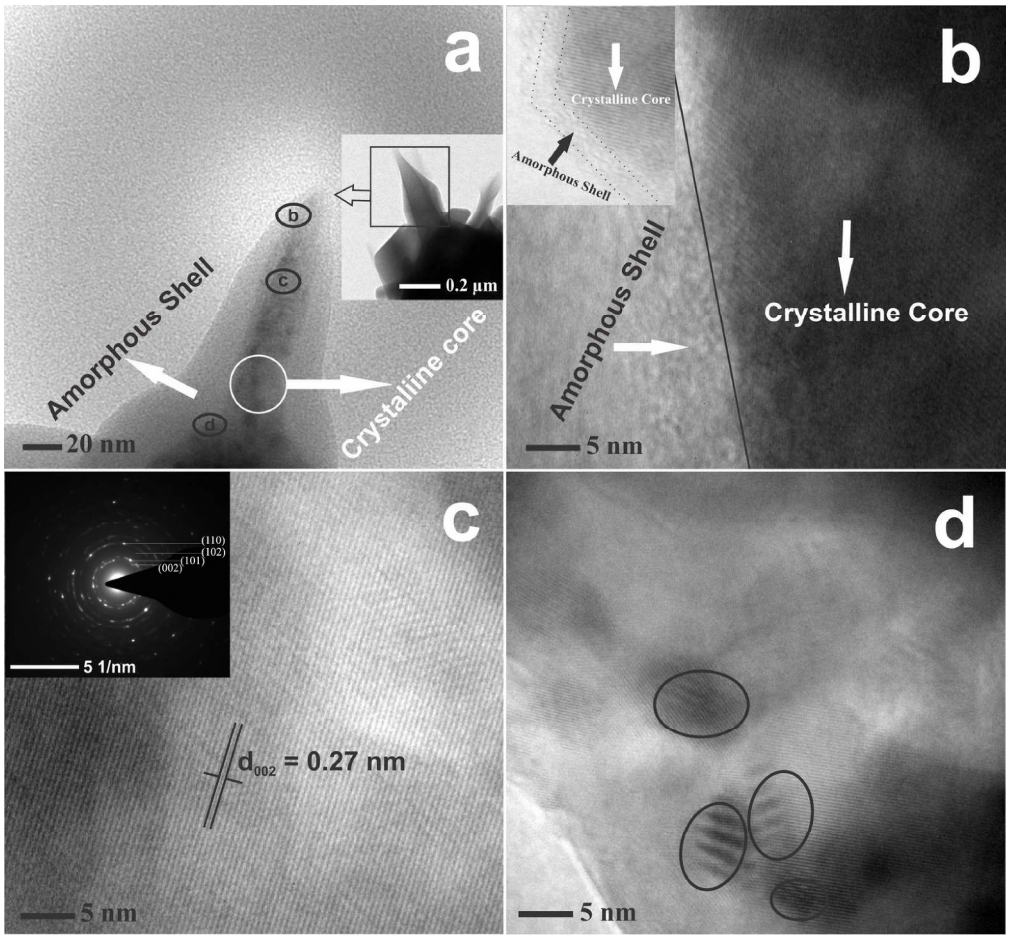

423x393mm (300 x 300 DPI)

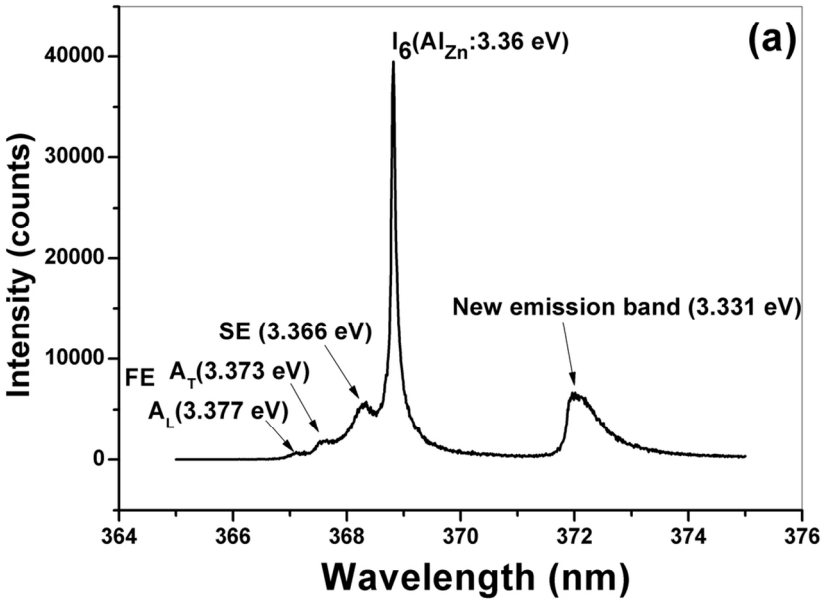

Low temperature (13 K) PL spectra of ZnO-ZnO core-shell nanorods (a) near band-edge region showing new emission band at 3.331 eV and (b) visible region showing structured green band emission.
57x40mm (600 x 600 DPI)

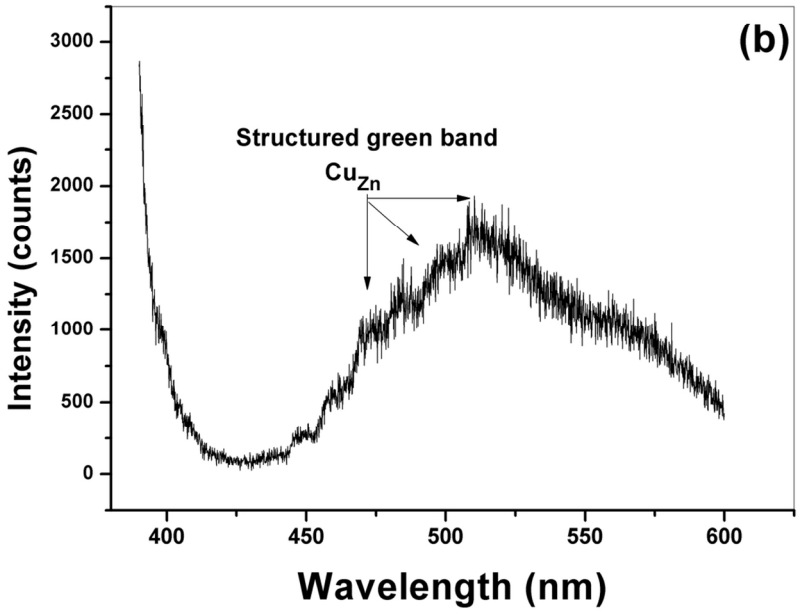

Low temperature (13 K) PL spectra of ZnO-ZnO core-shell nanorods (a) near band-edge region showing new emission band at 3.331 eV and (b) visible region showing structured green band emission.
57x40mm (600 x 600 DPI)

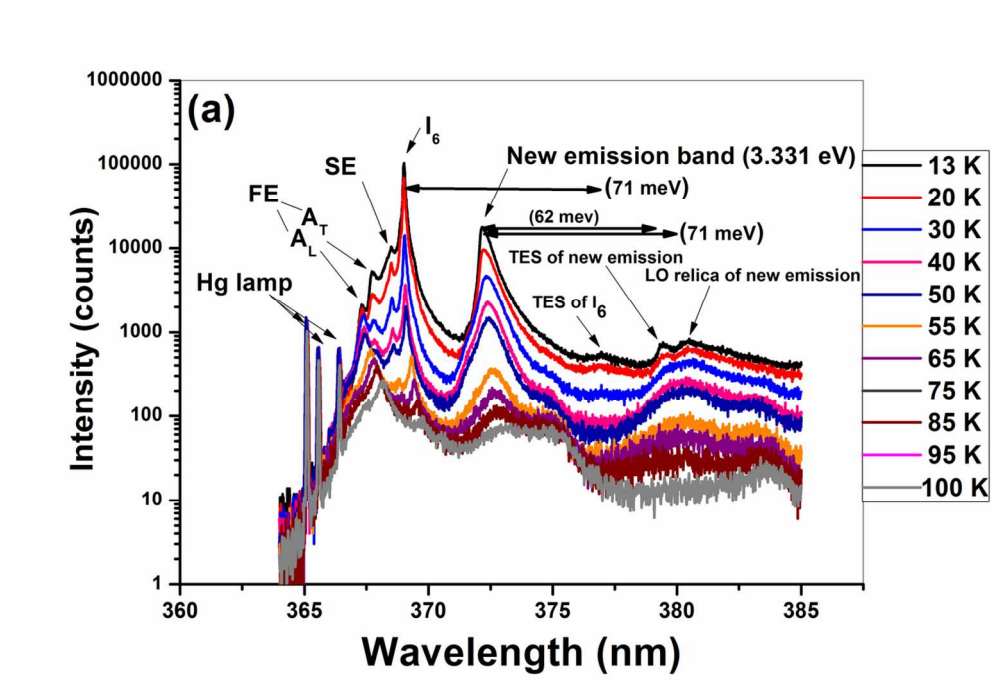

59x41mm (600 x 600 DPI)

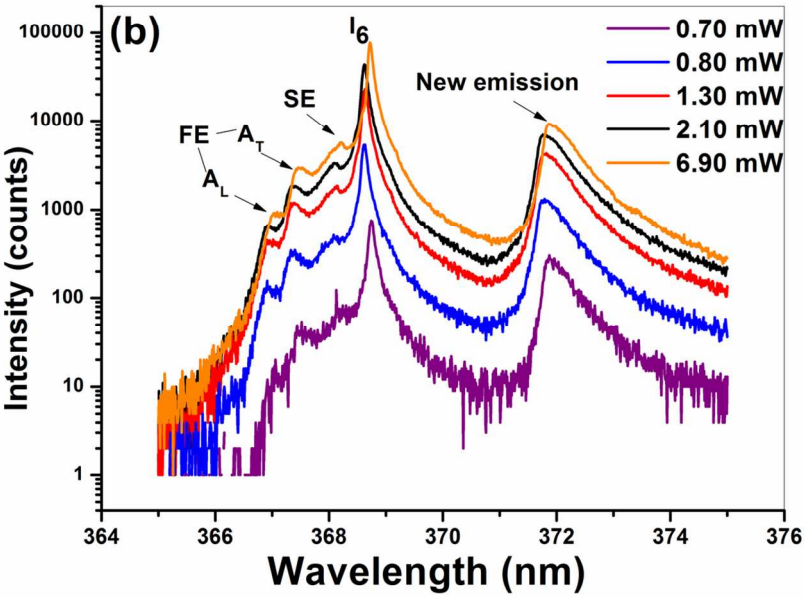

59x41mm (600 x 600 DPI)

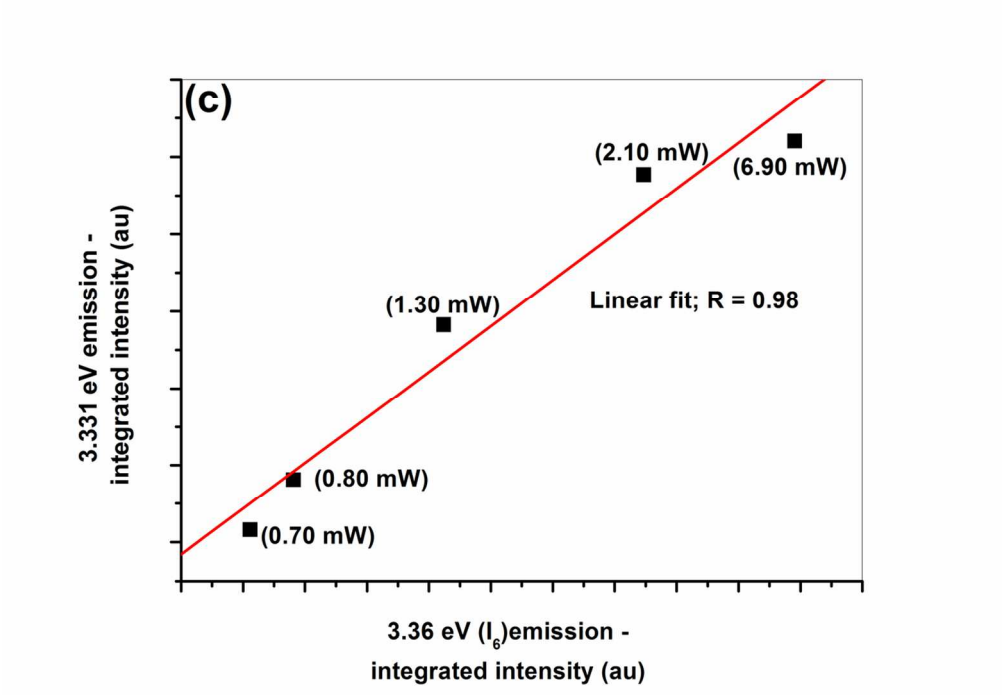

59x41mm (600 x 600 DPI)

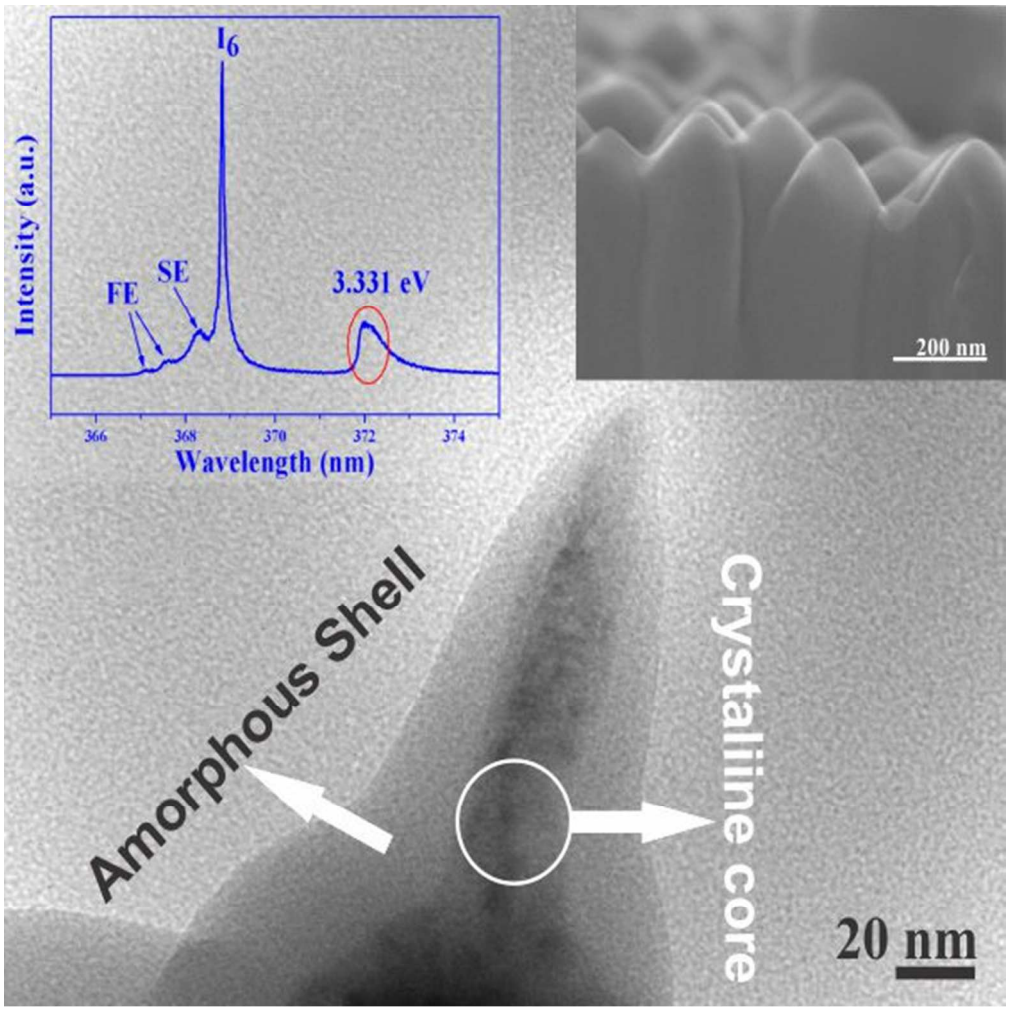

TOC
50x50mm (300 x 300 DPI)